IEEE Access
Multidisciplinary | Rapid Review | Open Access Journal

Received October 18, 2019, accepted November 30, 2019, date of publication December 16, 2019,
date of current version December 23, 2019.

Digital Object Identifier 10.1109/ACCESS.2019.2959810

A Deep Artificial Immune System to Detect Weld Defects in DWDI Radiographic Images of Petroleum Pipes

CELIA CRISTINA BOJARCZUK FIORAVANTI[1,2], TANIA MEZZADRI CENTENO[1], AND MYRIAM REGATTIERI DE BIASE DA SILVA DELGADO[1]

[1]Graduate Program in Electrical and Computer Engineering (CPGEI), Federal University of Technology of Paraná (UTFPR), Curitiba 80230-901, Brazil
[2]Department of Electrical Engineering (DAELT), Federal University of Technology of Paraná (UTFPR), Curitiba 80230-901, Brazil

Corresponding author: Celia Cristina Bojarczuk Fioravanti (celiacristina@utfpr.edu.br).

The work of M. R. D. B. D. S. Delgado was supported by the National Council for Scientific and Technological Development (CNPq) through the Coordination for the Improvement of Higher Education Personnel (CAPES) under Grant 309935/2017-2.

ABSTRACT In recent years, research focused on (semi)automatic radiographic inspection methods has gained more attention. The present work proposes a method for detecting defects in radiographic images of welded joints of oil pipes. Real condition images obtained by the double wall double image (DWDI) technique usually present a lower quality when compared with images traditionally considered in many studies reported in the literature. First, the proposed approach detects discontinuities in DWDI radiographic images of welded joints, and then, based on a hybrid paradigm encompassing artificial immune systems (AIS) and deep learning (DL), it classifies each discontinuity as 'defect' and 'non-defect'. The proposed method performs two phases in the AIS module: early classification (based on negative selection) and evolving classification (based on clonal selection). In both phases, the pattern recognition task is performed using a set of features extracted from each discontinuity through a detector genetically encoded into immune cells. As an attempt to improve the classification performance, DL models (AlexNet and autoencoders) are incorporated aiming to increase the number of extracted features. Experiments performed on a set of 727 discontinuities show that the proposed approach achieves an Fscore of 70.7%, outperforming each of its modules running by themselves: AlexNet with Fscore = 64.86% and AIS with Fscore = 66%. Considering the challenges imposed by real conditions on image acquisition - and the low rates of false negatives -, results demonstrate that the proposed approach can be used to assist in inspection works when dealing with DWDI images.

INDEX TERMS Artificial immune systems, deep learning, radiographic images, discontinuities classification, defect detection.

I. INTRODUCTION

In petrochemical facilities, networks of fluid-conductive pipes are constructed by attaching pipes and other components by means of welded joints [1], [2]. These facilities are carefully designed to withstand critical conditions of temperature and pressure; however, failures can occur. Serious consequences can be avoided with careful monitoring by periodic inspection programs through nondestructive testing (NDT) [3]. NDT consists of procedures and methods for examining products and materials without interfering or altering their functioning [4].

The associate editor coordinating the review of this manuscript and approving it for publication was Gangyi Jiang.

Radiography is one of the most widely used NDT methods for detecting internal defects in welded joints, since the radiographic image is a permanent visible record of the material volumetric inspection [5].

Weld inspection is performed by certified operators [5], called 'weld inspectors' or 'laudist inspectors'. Due to the large quantity of images to be inspected, the work can be exhausting, thus affecting time and quality of the inspection process [2]. The correct interpretation depends essentially on the experience, knowledge, and visual accuracy of the inspector as well as on image quality [6]. The inspection process of industrial radiographs is, therefore, quite subjective, increasing the possibility of errors [2], [7]. For all the

previously mentioned reasons, there has been a trend toward developing automated techniques able to efficiently assist inspectors in detecting defects in welded joints.

Several researches [2], [8] – [28] have proposed automatic or semiautomatic methods for detecting defects in welded joints (weld beads) from radiographic images. Most researchers use images obtained by the single wall simple image (SWSI) technique. A few works [24]–[28] address Double Wall Double Image (DWDI) exposure and they differ from one another in the way they use the images and the final goal of the work (*weld x defect detection x both*).

The present work uses real world DWDI radiographic images and a previously published procedure [26] to detect discontinuities. Additionally, it proposes a method based on Artificial Immune Systems (AIS) and deep learning to classify such discontinuities as 'defects' and 'non-defects'. The AIS mechanisms considered in this paper are 'negative selection' and 'clonal selection'. Aiming to improve the classification performance, the proposed approach incorporates deep learning models (AlexNet and autoencoders) to expand the number of extracted features beyond those initially obtained by AIS.

In addition to AIS's main characteristics of memory, diversity, and reinforcement learning capacity, the reason for choosing AIS is also based on its known capability of recognizing anomalies and internal and external patterns of the system.

On the other hand, some significant contributions have recently been achieved through the use of deep learning-based methods, mainly by doing feature extraction using Convolutional Neural Networks (CNN) [29]. However, due to the huge quantity of computational resource necessary to train CNN models from scratch, for the present paper it was decided to explore the use of transfer learning (TL). Besides saving training time, TL can also be used to overcome the lack of training samples in different application domains. Zhuang *et al.* [30], for example, uses an algorithm based on autoencoders to find a good representation of instances in different domains. Yosinsk *et al.* [31] and Oquab *et al.* [32] use a CNN as a generic feature extractor that is pre-trained using ImageNet data set and then reused for other tasks. Inspired by the literature, the present paper (i) uses an AlexNet model pre-trained with ImageNet data set and (ii) fine-tunes its full connected layers to perform two different tasks: deep features extraction and whole classification. Therefore, first, AlexNet is used in the proposed approach to provide additional features that are further compacted through the use of two autoencoders; second, in the experiments, it is considered as a unique module performing the whole classification task, which is further compared with the proposed approach.

The approach proposed in this paper is named 'deep AIS' and is inspired by both, human activities performed by inspectors and the basic functioning mechanisms of the biological immune system associated with artificial immune therapies. First, deep AIS preprocesses the image, investigating the regions of attention (discontinuities). Then it separates discontinuities that can be clearly classified as non-defects and defects. For this, it uses the mechanisms of censoring and monitoring performed by the negative selection algorithm. Then the system starts the clonal selection phase aiming to improve the classification. To this end, first, it tries to improve data through evolution by using lenses-like transformations performed by decoders located in the B cells (antibodies). Second, it reduces, from time to time, the threshold value necessary to classify a discontinuity as a defect aiming to reduce the false negative rates as much as possible. The experiments consider a set of 20 images of DWDI obtained in real conditions which result in a set of 727 discontinuities to be used in the training, validation, and testing phases.

The present work aims to evaluate two main hypotheses that also represent the two main contributions of the proposed approach: 1) using a dynamic threshold whose value decreases from time to time in the AIS module is better than using a fixed one, set with a low value from the beginning of evolution; 2) using the hybrid approach is better than using its standalone versions. For testing the first hypothesis, the experiments compare the static with the dynamically set threshold versions on a set of validation data. To test the second hypothesis, the deep AIS (hybrid version) is compared with two other methods (pure AIS and pure deep learning approach - AlexNet) on the test set.

The article is organized as follows: Section II presents a brief description of the fundamental concepts necessary to comprehend the proposed approach. Section III describes the related works. Section IV details the method proposed to detect defects in welded joints. Section V presents the results obtained with real field images. Finally, Section VI concludes the paper and presents suggestions for future works.

II. BACKGROUND

A. DOUBLE WALL DOUBLE IMAGE TECHNIQUE

The DWDI technique is used in pipes with a $3^{1/2}$ diameter or less that do not allow internal access [33]. In this technique, the source is positioned slightly away from the pipe and the radiation beam passes through both walls, producing an image of the two pipe sections. The radiation source can be positioned in two ways: aligned to the weld bead or slightly inclined. When the source is aligned to the weld bead, the weld bead projections of the two pipe walls are overlapped. When the source is positioned with an inclination of 12 to 15 degrees, projections of the two pipe walls result in an elliptical image (Figure 1).

B. ARTIFICIAL IMMUNE SYSTEMS

Similar to Evolutionary Computation, Artificial Immune Systems (AIS) are inspired by nature (more specifically, Biological Immune Systems), aiming to simulate mechanisms and create artificial systems for solving complex problems [34]. Research on AIS is extensive, and the choice of the best mechanisms/models depends on the objective and the addressed problem. Unlike other bio-inspired techniques, which usually

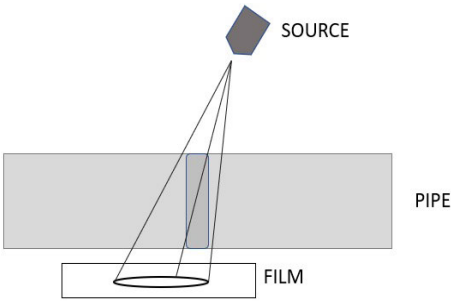

FIGURE 1. DWDI technique.

have a unique general algorithm, in AIS there is no general scheme of what essential elements an algorithm should possess.

The Immune System protects the body against infections originated from the attack of a disease-causing agent. Cells and molecules that do not belong to the body are recognized and eliminated [35]. Therefore, pattern recognition, which encompasses the defect detection problem addressed in the present paper, appears as a main application of AIS.

Every element that can be recognized by the immune system is called an 'antigen' (Ag). Cells that originally belong to our body and are harmless to its functioning are termed 'self' (or self-antigens), while the disease-causing elements are named 'nonself' (or 'nonself antigens') [36].

Among several already studied AIS models, this work uses clonal selection and negative selection, considering that both have specific characteristics for the pattern recognition task performed here.

1) NEGATIVE SELECTION ALGORITHM (NSA)

NSA [37] is an algorithm based on the pattern recognition process performed by the natural immune system, which classifies T lymphocytes within the thymus as self (known) and nonself (unknown) cells [38], [39], [40]. Defining the repertory of self cell patterns, the negative selection algorithm generates a set of detectors capable of identifying all elements that do not belong to the self cell set. As depicted in Figure 2, the algorithm runs in two phases as described below [36]:

a: CENSORING

- Define the set of self standards (S);

- Randomly generate a set of candidate samples (C) and evaluate the affinity (match) between each sample and the set of self standards. If an element of set S is recognized by a sample in C, that is, if the affinity is greater than a certain value (called 'self threshold'), delete the sample of C; otherwise, store it in a set of detectors (R).

After the R detector set is generated, system monitoring is performed to detect nonself elements.

b: MONITORING

- For all elements in R, given the chain set to protect (protected chains), evaluate the affinity between each of them and the R detector set. If the affinity is greater than a certain threshold, then a nonself element has been identified.

2) CLONAL SELECTION ALGORITHM (CSA)

This algorithm is based on the biological clonal selection principle [41], [38] and is initially proposed to solve machine learning and pattern recognition (antigen) problems where there is a random population of antibodies evolved to learn how to recognize a set of antigens. Antigens are the elements of the set of pattern templates, and antibodies are the elements of the set of possible solutions [42], [43].

The CLONALG algorithm developed by De Castro [44] encompasses the principle of clonal selection and affinity maturation and can be explained by the following steps:

1. Start with a set of antibodies;
2. Present each antibody to antigens and calculate an affinity measure (fitness function);
3. Select Antibodies with the highest affinities to antigens to be cloned in proportion to their affinities: the higher the affinity, the greater the number of clones;
4. Submit clones to the affinity maturation process; each one mutates at a rate inversely proportional to its affinity: the higher the affinity the lower the mutation rate;
5. Calculate the affinity between the set of mutated clones and antigens. Mutated clones with higher affinity values replace antibodies with lower affinity introducing diversity into the repertoire;
6. If the number of iterations is complete, finish the algorithm; otherwise, return to step 2.

In each iteration, the CLONALG algorithm allows the artificial immune system to become increasingly better to perform the pattern recognition task.

According to Dasgupta and Gonzalez [38], this algorithm resembles evolutionary algorithms based on mutation with some interesting features, such as: dynamically adjustable population size, exploration of the search space, ability to maintain optimal local solutions, and defined stopping criteria.

C. DEEP LEARNING

1) CONVOLUTIONAL NEURAL NETWORKS (CNN'S)

The convolutional neural network [45] is a multilayer perceptron network specifically designed to recognize two-dimensional shapes with a high degree of translation invariance, scaling, tilting (rotating), and other forms of distortion [46].

CNN's are formed by layer sequences and each layer has a specific function in propagating the input signal. Figure 3 illustrates the architecture of a specific CNN - named AlexNet [47] - and its three main layers: convolutional, pooling, and fully connected layers (FC).

Convolutional layers extract attributes from input volumes (3D size), which are images with width, height, and depth (RGB). Pooling layers reduce the dimensionality of the resulting volume after convolutional layers and help render the representation invariant to small input translations.

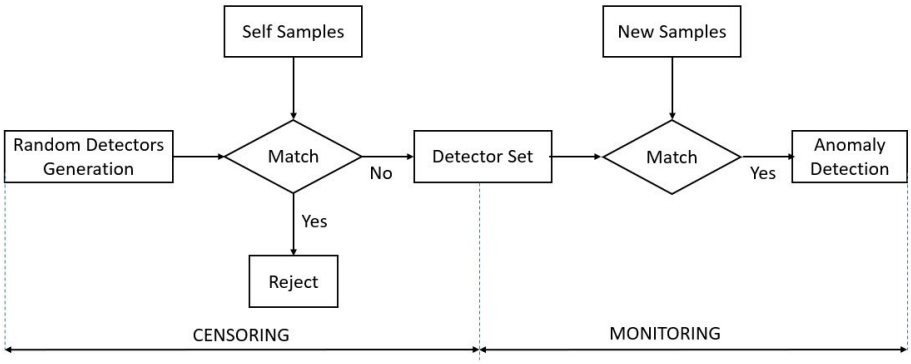

FIGURE 2. Negative selection algorithm. Source: Adapted from [37].

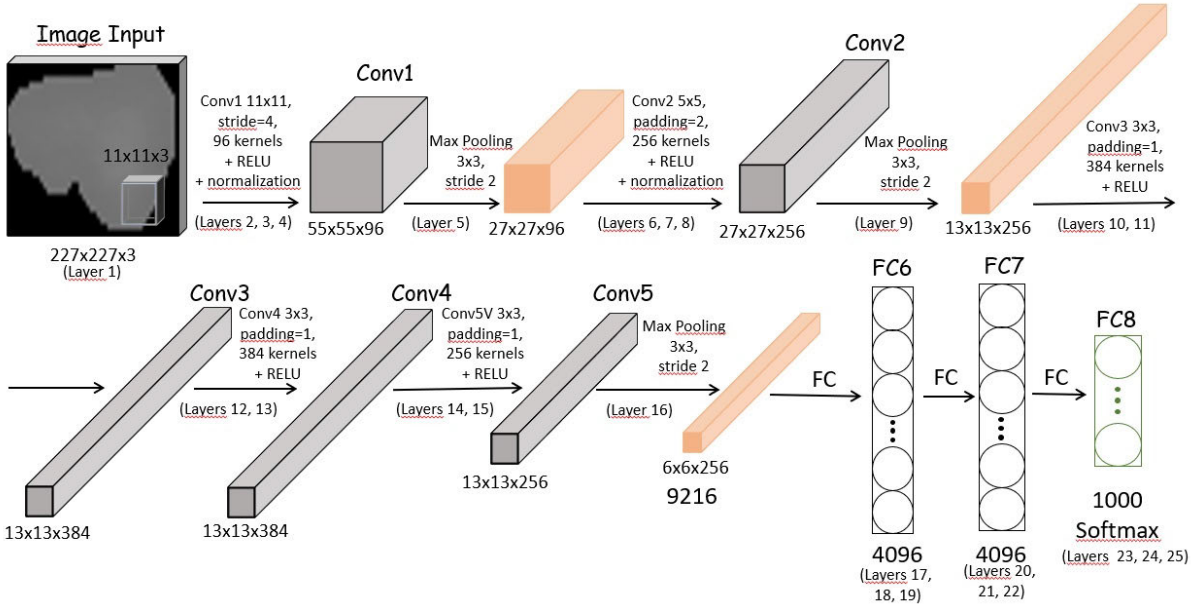

FIGURE 3. Example of CNN architecture, AlexNet, with their respective layers. Source: Adapted from [47].

Fully connected layers (FC) are responsible for signal propagation through peer-to-peer multiplication and also use an activation function. CNN output is the probability that the input image belongs to one of the classes the network was trained to detect.

a: CONVOLUTIONAL LAYER

Convolutional layers are composed of a set of filters (kernels) able to learn from training. Each filter has a small size but extends throughout the depth of the input image. Automatically, during the net training process, these filters are adjusted so that they are activated in the presence of relevant features identified in the image, such as edge orientation or color spots [48]. Each of these filters gives rise to a locally connected structure that runs the full length of the image, an operation known as 'convolution'. The resulting values after the convolution operation go through an activation function - the ReLU (Rectified Linear Units Units) function being the most common [48] - which can be calculated by Equation (1).

$$f(x) = max(0, x) \tag{1}$$

To control the size of the image resulting from the convolutional layer, there are three parameters: depth, stride, and zero-padding [49]. The resulting image depth is equal to the number of filters used, and each of these will be responsible for extracting different characteristics from the input image. Therefore, the higher the number of filters, the greater the number of features extracted, but the computational complexity related to time and memory use will also be greater.

The resulting image depth depends only on the number of filters used, while the resulting image's height and width depend on stride and zero-padding. The stride or step specifies the size of the jump in the convolution operation. The higher the step value, the smaller the height and width of the resulting image will be, but important features may be lost. For this reason, it is unusual to use a jump value greater

than two. Zero-padding is a technique that allows preserving the size of the original image by adding a pixel border to the input image, and all with the value zero.

b: POOLING LAYER

After a convolutional layer, there is usually a pooling layer. The purpose of this layer is to progressively reduce the spatial dimension of the input image and, consequently, decrease the computational cost of the network and avoid overfitting [48]. In pooling, values belonging to a region of the attribute map, generated by convolutional layers, are replaced by some metric for that region. The most common form of pooling is to replace the values of a region with the maximum value [50]. This operation is known as maxpooling and is useful for eliminating negligible values, reducing the size of the data representation, and accelerating the computation required for the next layers. Besides, it creates invariance for small local changes and distortions. Note that the depth of the input volume is not altered by the pooling operation.

c: FULLY CONNECTED LAYER

The output of the convolutional and pooling layers represents the characteristics extracted from the input image. The purpose of the fully connected layer is to use these features to classify the image into a predetermined class. Fully connected layers are exactly the same as a conventional Artificial Neural Network (Multi Layer Perceptron or MLP) [51] that uses the SoftMax activation function [52], defined by Equation (2), on the last layer (output).

$$S(y_i) = \frac{e^{y_i}}{\Sigma j e^{y_i}} \tag{2}$$

where yi represents the input of neuron i, and $S(y_i)$ represents its output. The expression 'fully connected' means that all neurons in the previous layer are connected to all neurons in the next layer.

The SoftMax activation function receives a set of values as input and produces the probabilistic distribution of the classes in which the network was trained. A technique known as 'dropout' [50] is also widely used between fully connected layers to reduce training time and avoid overfitting. This technique consists of removing - randomly in each training iteration - a certain percentage of neurons from one layer and then re-adding them to the next iteration. This technique also gives the network the ability to learn more robust attributes, since a neuron cannot depend on the specific presence of other neurons.

2) ALEXNET ARCHITECTURE

AlexNet, proposed by Krizhevsky *et al.* [47], is a basic, simple, and effective CNN architecture composed mainly of cascading stages of convolution layers, ReLU activation function, maxpooling, dropout layers, and fully connected layers, totaling 25 layers presented in Table 2 - in the Appendix.

In this architecture, filters are obtained during the training phase based on optimization routines with the Stochastic Gradient Descent (SGD) algorithm. Convolutional layers typically act upon input of feature maps with sliding filters to generate convoluted feature maps. As discussed in the previous section, pooling layers operate on convoluted feature maps to aggregate information from within the neighborhood region provided with a maxpooling operation. Another characteristic of AlexNet consists of some practical strategies, such as the ReLU activation function and dropout technique.

As will be discussed in Section IV, the AlexNet model is used to expand the set of characteristics to be used in the AIS matching process. In this case, the layer just before the full connected layer is the output of a cascade of two autoencoders used to reduce the dimensionality of the extra feature vector. In Section V - in the comparison test - AlexNet is adapted to perform a 2-class classification task in a standalone mode.

3) AUTOENCODER

Autoencoder is a multilayer neural network with a minimum of three layers whose output layer is defined with the same number of nodes as the input layer [53], [54]. It has the purpose of learning how to reproduce on output y its own input data x. Internally, the network has a hidden layer h describing a code used to represent the input. The network can be understood as containing two parts: the encoder having function $h = f(x)$, and the decoder having function $r = g(h)$; thus, the autoencoder can be described by the function $g(f(x)) = r$ [55].

Figure 4 presents an example of autoencoder that reduces the dimensionality while maintaining the main information. The hidden layer is smaller than the input layer and can have multiple layers.

The hierarchical levels of data representation - low and high levels - can be organized by abstractions, characteristics, and concepts. For example, low-level features that are invariant to small geometric variations (such as edge detectors from Gabor filters), gradually transform such resources (e.g., to make them invariant to contrast changes and contrast inversion) in order to subsequently detect the most frequent patterns and obtain high-level resources [56].

A single layer network can extract resources seen as low level, but by adding a second layer and the output of the first being input of the second, the extracted resource may be of slightly higher level [56]. Therefore, the output generated by the hidden layer training of the first autoencoder becomes the training input of the second autoencoder and, therefore, a new pre-training is performed by the second autoencoder. The output generated by the hidden layer of the second autoencoder is the high-level characteristics.

D. MORPHOLOGICAL IMAGE PROCESSING

The basic principle of mathematical morphology is to extract geometry and topological information from an unknown set (an image). This is performed by transforming the input through another completely defined set, called the 'structuring element' (SE). Figure 5 presents some examples of structuring elements. In this figure, the darkest point indicates

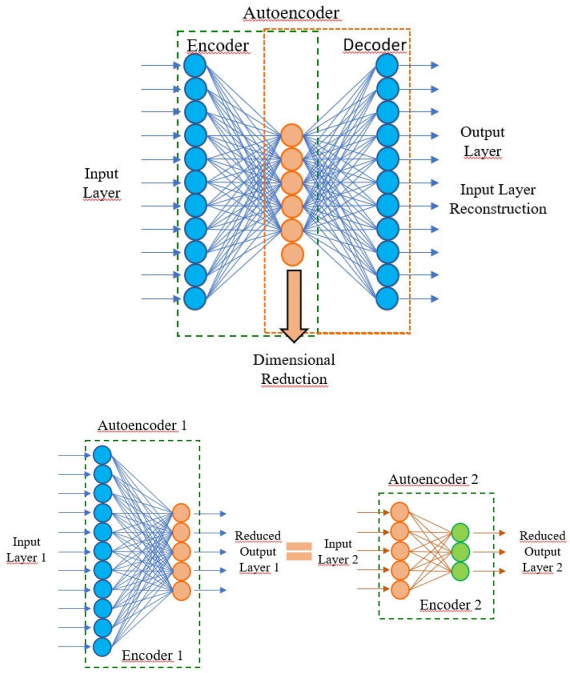

FIGURE 4. Autoencoder scheme used for dimensional reduction. Source: Adapted from [54].

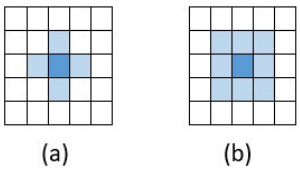

FIGURE 5. Example of structuring elements. (a) Cross 3×3. (b) Square 3×3. Source: Adapted from [57].

the origin of its coordinate system, i.e. the position of the pixel the result will be assigned to [57].

Morphological operations act on the neighborhood of a certain pixel, the shape and size of which are determined by the superposition of the SE on each pixel of the image. The new value of each image pixel depends on the pixel values in the SE-defined neighborhood [57].

1) MORPHOLOGICAL OPERATIONS OF EROSION AND DILATION

Erosion is defined by Equation (3), where A is the input image (Figure 6(a)), and B is the SE. Thus, $A \ominus B$ results in the set of points x such that B, translated from x, is contained in A [57] (Figure 6(b)).

$$A \ominus B = \{x|(B)_x \subset A\} \tag{3}$$

Dilation is obtained through Equation (4). The dilation process consists of obtaining the reflection of B about its origin and then displacing this reflection of x. The expansion of A by B is then the set of all x offsets for which the intersection of $(\hat{B})_x$, and A includes at least one nonzero element so that B and A overlap at least by one element [57].

FIGURE 6. Example of morphological operations. (a) Input image. (b) Eroded image. (c) Dilated image.

Figure 6(c) illustrates the result of morphological operation dilation.

$$A \oplus B = \{x|(B)_x \cap A \neq \emptyset\} \tag{4}$$

E. PERFORMANCE MEASURES

A classifier can have its performance evaluated by several methods. The effectiveness of a classification can be assessed as: number of correctly recognized class samples (true positives); number of samples that were correctly assigned as not belonging to the class (true negatives); samples that were incorrectly assigned to the class (false positives); and, finally, samples that were incorrectly classified as not belonging to the class (false negatives).

Sokolova and Lapalme [58] and Powers [59] carry out studies to prove that, with the confusion matrix, there are some statistical results such as accuracy, sensitivity, and precision. These results are calculated as a function of true and false positive and negative values, as follows:

- Accuracy: Calculated by the ratio between the total number of samples that are correctly classified and the total number of samples (Equation 5).

$$Accuracy = \frac{TP + TN}{TP + TN + FP + FN} \tag{5}$$

- Precision: Calculated by the ratio of the number of true positives to the total of samples classified as positive (Equation 6).

$$Precision = \frac{TP}{TP + FP} \tag{6}$$

- Sensitivity: Calculated by the ratio of the number of true positives to the number of truly positive samples (Equation 7).

$$Sensitivity = \frac{TP}{TP + FN} \tag{7}$$

- Fscore: Calculated by the weighted average of precision and sensitivity (Equation 8). The Fscore measure is indicative of the overall performance of the classifier. This statistical measure is often the combination of precision and sensitivity.

$$Fscore = \frac{2x(Precision \times Sensitivity)}{(Precision + Sensitivity)} \tag{8}$$

III. RELATED APPROACHES

Most studies presented in the literature for detecting weld defects consider radiographic images obtained through the SWSI technique. Among those works, many researchers initially perform digital processing to reduce noise and improve

quality according to each image. Subsequently, they perform the extraction of the weld bead, as well as the extraction and classification of defects. Most traditional approaches include different models of neural networks ([10], [12], [20], [60]), neural network combined with binary logic ([13]), surface thresholding method ([61]), neuro-fuzzy (ANFIS) ([19]), support vector machine (SVM) ([22]), as well as approaches with more than one model like fuzzy, KNN and neural networks ([9]); minimum distance, KNN and fuzzy KNN ([14]); SVM, neural networks and KNN ([18]).

There are few studies reported in the literature based on the DWDI exposure technique, and they are presented below. Four of them on weld detection [23]–[28] and only one [26] on defect classification.

Rathod and Anand [23] develop a method based on genetic algorithm (GA) for detecting weld bead in radiographic images obtained by the DWDI technique. Sets of sample pixels, corresponding to candidate solutions provided by a genetic algorithm (GA), are compared to pre-defined synthetic weld bead models in an image matching procedure. The evolutionary process automatically selects the best individual in the population and, thus, provides information such as position, orientation, and dimension of the detected object. This approach successfully detects pipes and weld beads in radiographic images of different complexities.

Suyama *et al.* [25] present a methodology to detect the central region of weld beads in DWDI radiographic images. The method is based on three steps: pre-processing (isolating selected regions), optimization (defining the ellipse that best fits the selected region), and decision (choosing the best region based on its extracted features). The results show that the Particle Swarm Optimization (PSO) algorithm satisfactorily converges to select the region that is most similar to the central weld region in the optimization and decision steps. The authors conclude that the proposed technique can work as a support for detection and extraction of weld in DWDI radiographic images.

Miranda *et al.* [27] present an automatic weld bead detection approach in DWDI radiographic images, combining two known techniques: Particle Swarm Optimization (PSO) and Dynamic Time Warping (DTW), which is suitable for handling comparison between series of different sizes. PSO-based optimization is responsible for extracting the image profile. The quality calculation of each solution is based on a comparison with the synthetic profile model and considers the cost function calculated by the DTW. A fine-tuning process is used as an attempt to find a better similarity profile after the PSO search is completed. Similar to the conclusions of [25], the proposed approach can support professionals by automatically segmenting weld beads to further performed defect detection.

Suyama *et al.* [26] develop an algorithm for automatic detection of weld bead discontinuities using image processing techniques and ensembles of classifiers with Multilayer Perceptron and special models of NN called Extreme Learning Machines. A set of characteristics (features) is extracted from the detected discontinuities to be used as the classifier input. These features are also extracted and used in the approach proposed in this paper. For each discontinuity, there are eight geometric shape features and five texture features. For each discontinuity, one has the following geometric shape characteristics:

1. Area (A): area of discontinuity (defect) detected, i.e. total number of pixels within the discontinuity, including its outline;
2. Extension ($E_x = A/A_r$): ratio between the area of the defect and the area of the smallest rectangle surrounding the defect;
3. Ratio 1 ($R_1 = d/A$): ratio between the smallest axis of the rectangle surrounding the defect and the defect area;
4. Ratio 2 ($R_2 = D/A$): ratio between the largest axis of the rectangle surrounding the defect and the defect area;
5. Ratio 3 ($R_3 = D/d$): ratio between the largest axis and the smallest axis of the rectangle surrounding the defect;
6. Rounding: ratio ($p^2/4.\ \pi.\ A$), where p is the perimeter of the defect contour and A is the defect area;
7. Eccentricity ($E_c = c/a$): ratio of the distance between the foci of the ellipse and its major axis length;
8. Solidity ($S = A/A_c$): ratio between the area of the defect and the convex polygonal area of the defect.

For each discontinuity, one has the following texture characteristics:

1. Difference ($D = max\_gray\_level - min\_gray\_level$): difference between the lowest and highest gray level of the defect;
2. Contrast ($C = D - gray\_variation$): ratio between the gray level variation in the defect and the gray level variation in the image crop;
3. Standard deviation (Equation 9): measure of dispersion in relation to the average gray level of the defect, where N is the number of pixels, B is the gray level and i is the level position;

$$\sigma = [(\Sigma_{i=1}^{N} | B_i - \dot{B}|^2)/(N-1)]^{1/2} \quad (9)$$

4. Entropy ($E = -\Sigma(p.\ log2\ (p))$): Quantifier number of the grayness randomness of the defect. The higher this number is, the more irregular, atypical or unpatterned the analyzed image will be.
5. Asymmetry ($s = E.\ (x-\mu)^3/\sigma$): Asymmetry regarding the center of the gray level values of the defect, where x is the input data, μ is the mean of x, σ is the standard deviation of x, and $E(t)$ represents the expected value of the quantity t.

Suyama *et al.* [28] present a methodology to detect weld joints of oil pipelines in radiographic images with DWDI exposure. The proposed approach extracts information (windows of pixels) from the pipeline region in the radiographic image and then applies Deep Neural Network (DNN) models to identify which windows correspond to welded joints. The experiments consider 13 DNN models and 3 DNN input

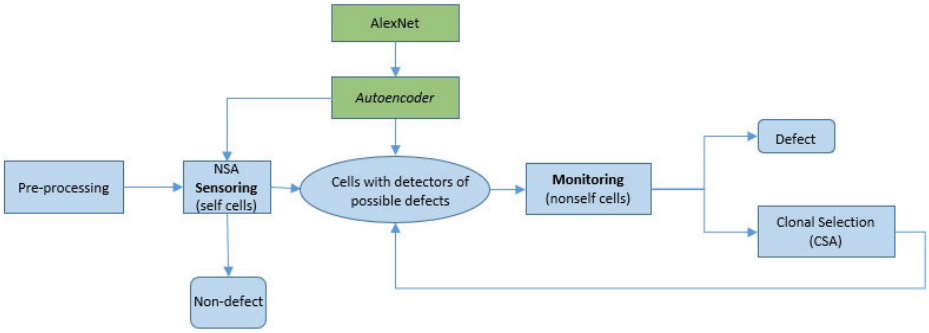

FIGURE 7. Overview of the proposed approach: deep AIS.

settings: stretched, proportional, V and proportional H. Similar to the conclusions of [25], [27], the proposed approach can also support professionals by automatically segmenting weld beads to further performed defect detection.

Based on the related approaches review, it is pointed out that many works for the detection of weld defects in radiographic images are presented in the literature; however, few researchers work on radiographic images obtained through the DWDI technique, most on the identification of the weld, and quite few on the detection of defects. In addition, many works use ideal images rather than real field images, which are generally low quality images. Besides, for classification purposes, most researchers use only one system (Neural Networks) for pattern recognition. Thus, the present work applies some image processing techniques, such as: noise reduction filters, histogram, equalization, morphological operations, among others, to highlight existing weld bead discontinuities. For the classification of a discontinuity as defect or non-defect (pattern recognition), two techniques are used in the same model: deep learning and AIS. The choice for AIS is based on its main characteristics (uniqueness, recognition of internal and external patterns of the system, anomaly detection, imperfect detection, distributed detection, diversity, reinforcement learning, memory) [35], [36]. The approaches presented in the present paper are not compared to Boareto's [26] approach to defect classification, since his work was tested on other bases and the authors did not have access to the code.

On the other hand, deep learning has been successfully applied to a lot of pattern recognition tasks like the one performed in this paper, although only one work has been found dealing with radiographies of petroleum pipes [28].

IV. DEEP AIS

For the classification of discontinuities detected in a pre-processing phase, a hybrid system joining artificial immune system and deep learning is proposed. As depicted in Figure 7, the AIS module (blue boxes) encompasses the Negative Selection Algorithm (NSA) and Clonal Selection Algorithm (CSA), and is used to:

1. separate self cells (non-defects detected in the censoring phase of NSA);
2. separate nonself cells (defects detected in the monitoring phase of NSA);
3. evolve, by means of CSA, antibodies aiming to improve detection of nonself elements.

The deep learning module (green boxes in Figure 7) encompasses two neural models (AlexNet and autoencoder) and is used to extend the number of features used in the matching phase of NSA and CSA.

Initially, in the pre-processing phase, discontinuities are detected in the weld bead cut-out images. Discontinuities are identified by the (x, y) coordinates of their centroid, and their limits are based on their borders, which are obtained through image processing techniques (see [26] for more details). As will be detailed in the next section, the discontinuity size defines the class of possible defects into two classes: large and small ones.

Subsequently, the method extracts features from each discontinuity encompassing window. Two databases are then constructed: the set of non-defects and the set of defects. Part of non-defect set composes the bank of self cells, and part of defect composes the bank of nonself (called 'antigen bank'). The other part composes the set of samples used in the validation and test phase. One of the main challenges in this work is the lack of data to compose training, validation, and test set, the labeling of which depends on oil pipe experts.

A. AIS MODULE

As illustrated in Figure 7 and detailed in Figure 8, the AIS module is composed of negative selection and clonal selection algorithms whose basic components are the T and B cells. In the context of this application, each T cell represents a set composed of a detector, AIS, and deep features; and each B cell is similar to a T cell (they differ only in the detector genetic encoding, since B cells consider all the detector alleles, and T cells disregard the last two genes: morphological operator (MO) and structuring element (SE)) (see Figure 9 for more details).

The first step is performed by Negative Selection Algorithm (NSA). By recognizing its own elements, it eliminates discontinuities clearly representing non-defects. For this, NSA calculates the affinity between the T cell representing the pre-detected discontinuity and each cell stored in the self

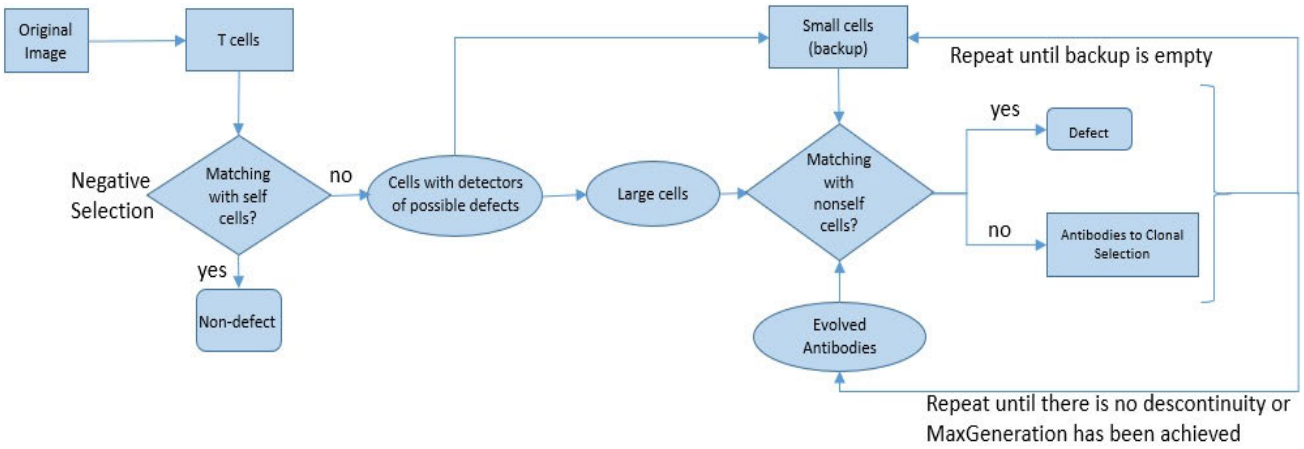

FIGURE 8. Pure AIS system proposed for the recognition phase.

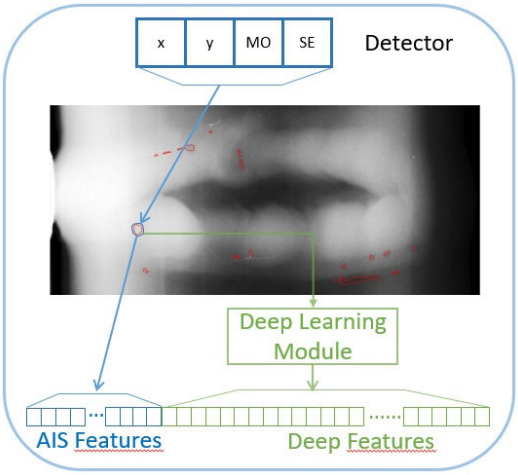

FIGURE 9. Example of T or B cell (antibody) leveraged by deep learning (in green).

repository (bank of self). As will be detailed in the clonal selection phase, the affinity is calculated based on a distance metric between feature vectors of both cells.

A discontinuity is recognized as non-defect if it matches one of the cells present in the self repertory. In other words, it is recognized if its affinity with a self cell is higher than the threshold of self (γ_s). A high value for γ_s must be set for negative selection so that only discontinuities strongly characterized as non-defects are excluded from the process.

In NSA, cells that match self cells are eliminated, and their associated discontinuities are labeled in the original image. Discontinuities not associated with self cells, i.e. those that are not eliminated by NSA, are possible defects and must be further analyzed using the antigen bank. The set of possible defect cells is divided into two groups: large and small cells. As depicted in Figure 8, the large group goes directly to be used in the nonself matching phase. The second one is stored in the system backup for further analysis.

During the nonself testing phase, the current set of cells under analysis is compared with the antigen bank, for

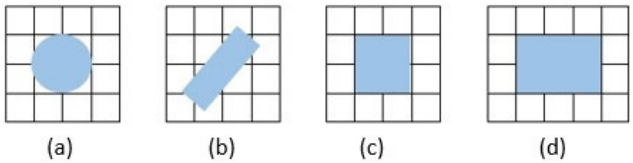

FIGURE 10. SE's used. (a) Disk of radius 1. (b) Line with length 3 and angle 45°. (c) 2×2 square. (d) 2×3 rectangle.

classification purposes. Cells classified as defects (i.e. those with affinity higher than the initial threshold, γ_d^0) have their discontinuities labeled and are excluded from the process. The remaining ones are still considered as potential defects and evolve based on the clonal selection algorithm (CSA), which is based on antibody evolution.

Each antibody has a detector (Figure 9) composed of the following genes:

- position of each discontinuity (x and y coordinates),
- a numerical value determining not only the morphological operator (erosion or dilation), but also the number of iterations that this operator will be applied to the discontinuity,
- a numerical value indicating which structuring element (SE) will be used in the morphological operation.

Thus, each antibody detector is represented by a set of genes encoding two localization alleles and two morphological alleles, as shown in Figure 9.

The values of x and y identify the position (line, column) of the discontinuity in the whole image. The value of the morphological operator (MO) can range from ($-$M to $+$M) M $\epsilon\mathbb{N}$ (natural numbers) allowing different variations. For example, -3 encodes three erosion iterations and $+3$ encodes three dilation iterations. The value of the structuring element (SE) may vary in the range (0 to $|\{SE\}|$) encoding an SE type or no SE (0). Some types that could be used for SE are shown in Figure 10: (1) disk of radios 1, (2) line with length 3 and 45° angle, (3) 2×2 square and (4) 2×3 rectangle.

In CSA, during the initialization of the population, each T cell gives rise to an antibody (see Figure 9) by randomly

setting MO and SE alleles values in the detector genetic encoding. In the proposed approach, besides the features extracted in the pre-processing phase that can be further improved by the evolved detector, the set can be expanded through the deep module as detailed in Section IV.B. In the proposed approach, at the first generation of CSA, there is a population P_{Ab} of antibodies that will evolve along C cycles of evolution. Each antigen in the antigen bank is also represented by its feature vector. However, unlike antibodies, antigen alleles do not change during the evolutionary process as well as their associated features, which remain fixed along all the process.

As previously mentioned, during the initialization of P_{Ab} population, alleles x and y define the position of the window used to extract the features and the other alleles (MO and SE) receive random values. During the cloning process, each antibody creates n clones of itself, each clone undergoes a hypermutation process that changes the alleles of its detector. Clonal selection controls the rate of hypermutation that is related to the affinity value. The higher the affinity, the lower the hypermutation rate is.

During the matching process that occurs at each generation of the clonal selection phase, affinities are calculated between each antibody and all antigens by Equation (10).

$$f_i = maxf(Ab_i, Ag_j) = max(1 - d_{ij}) \quad i = 1, \ldots, |P_{Ab}| \text{ and } j = 1, \ldots, |Ag| \qquad (10)$$

where $|P_{Ab}|$ is the total of individuals (antibodies) in the current population and $|Ag|$ is the cardinality of the set of antigens (antigen bank).

The affinity of each antibody i is given by the maximum affinity value between it and all antigens, and d_{ij} is any metric used to calculate the distance between feature vectors of antibody i and antigen j.

If f_i is greater than or equal to γ_d^c (that is, if f_i is greater than the defect threshold value that was set in the current cycle c of evolution), the antibody is considered a defect. Antibodies classified as defect have their associated discontinuity labeled in the original image and are suppressed from the evolutionary process. This elimination creates space for the analysis and further evolution of randomly chosen backup cells. Conversely, if the affinity does not exceed the γ_d^c value, the antibody remains as a potential defect and, by mutating its detector alleles, it can be classified as a defect (by matching one cell in the antigen bank) in further stages of the evolutionary process.

In the context of biological inspiration, aiming to improve the efficiency of the immune response upon close contact with antigens, antibodies of the P_{Ab} population go through cloning and hypermutation processes. In the context of image processing, one considers that the image of detected discontinuities does not always cover a defect due precisely to some detection failure. Therefore, antibodies evolution is like an attempt to allow an improvement in features extracted for classification purposes. To this end, hypermutation causes variations in the antibody detector genes (which in turn may cause variations in the discontinuity dimension and contour).

The detector genes perform like lenses, since they encode changes to be made by the way each discontinuity associated with the antibody is viewed (the original image is not altered). The goal is to enable the antibody to fit the antigens by transforming the detector genes aiming to improve the affinity value that classifies it as a defect. Thus, each discontinuity located at (x, y) coordinates has its dimensions and shape changed according to the detector gene values. An example of this transformation is shown in Figure 11.

(a) (b)

FIGURE 11. (a) Original discontinuity view. (b) Altered view with dilation +3 with SE radius disk 1.

In this example, MO and SE alleles are 3 and 1, respectively; therefore, the discontinuity undergoes three iterations of dilation with SE set as radius disk 1. Due to hypermutation, discontinuities can be subjected to different types of modification by combining MO and SE variations. The hypermutation step generates random antibody changes and helps the proposed algorithm to avoid local optimal values, creating a higher level of diversity.

In the proposed approach, the antibodies of the P_{Ab} population are evolved based on the steps shown in Figure 12.

The entire evolutionary process is completed when one of the following stopping criteria is met: there are no more discontinuities to classify or the maximum number of generations is reached.

B. DEEP LEARNING MODULE

As shown in Figure 7, the proposed deep AIS system for classifying discontinuities utilizes an AIS module, together with deep learning. The deep learning module has been included as an attempt to improve the defect classification performance by increasing the number of features to be analyzed.

In the proposed approach, two deep learning models (a CNN and an autoencoder) are plugged in into the AIS module to expand the information stored in the feature vector. This step is inspired by immune therapies present in some disease treatments in which the immune response is leveraged by external artificial mechanisms.

First, one considers the CNN AlexNet model - described in section II.C.2 - to extract features. Second, the autoencoder - described in section II.C.3 - is used to reduce the dimensionality of features extracted by CNN.

AlexNet considers 227 × 227 × 3 dimensions images (227 rows, 227 columns, and 3 color channels) [48] as input. Since the image window sizes of detected discontinuities may be incompatible with the image dimensions used by

Algorithm 1: Clonal Selection

```
While stop condition are not met
    For cycle c=1, …, C
        For gen = 1,…, MaxGenPerCycle
            Define Threshold value γ_d^c.
            Present each antigen to the current population of antibodies (P_Ab) and, using Eq. (10),
              calculate the affinity f_i for each antibody i ∈ P_Ab, i=1, …, |P_Ab|.
            Compare each f_i with the current defect threshold γ_d^c.
            If (f_i > γ_d^c)
                Label discontinuity located at the position (x, y) as defect and remove i from P_Ab.
                Randomly choose a small cell stored in backup (it is not empty) and create a new
                antibody from this small cell by randomly setting its MO and SE values.
                Include the new antibody in P_Ab.
            Clone all antibodies in P_Ab proportionally to their affinity values. This means generating
              n = |_fi _| clones for each antibody i, where |_ _| means 'floor function'.
            Hypermutate each clone aiming to improve its antibody detector.
            Update the features of the hypermutated clone as well as its affinity with the antigen
              bank.
            For each antibody i select the hypermutated clone with the highest affinity (best clone).
            Compare the affinity of the best clone with the affinity of its parent replacing it if the
              best is better.
            gen = gen + 1;
        end for gen
        c = c + 1;
    end for cycle
end
```

FIGURE 12. Pseudocode of clonal selection.

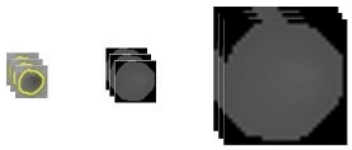

FIGURE 13. Extraction of discontinuity characteristics with AlexNet. (a) Image obtained from Antibody detector. (b) Dilated image with black border. (c) Image resized to fit AlexNet input dimensions.

AlexNet preliminary tests showed that some procedures on the discontinuity images must be performed before applying the necessary resize step (see Figure 13 and Figure 16 with the modified version of the AlexNet, described in the Section V.C).

For each discontinuity, an iteration of dilation is applied with the SE radius disk 5, and its encompassing rectangle is obtained. The region outside the discontinuity boundary is filled with gray level 0 (black) (Figure 13b) so that other elements present in the image do not influence the feature extraction. All discontinuity images are scaled to the size used by AlexNet, in both training and testing phases, and the channels are replicated so that all images have 3-channel (Figure 13c).

The first level of deep features is obtained at the first full connected layer, resulting in a vector with 4096 elements as described in section II.C.2. Figure 3, section II.C.1, and Appendix A show, respectively, the AlexNet model used in this paper and the detailed description of each layer, as well as the respective values of the parameters used.

Features extracted by the AIS module could be used in conjunction with the features directly obtained by AlexNet. However, some experiments showed that, due to the large number of characteristics obtained by AlexNet (4096 characteristics), this combination did not perform well. Thus, in the proposed deep AIS, the dimensionality of the feature vector obtained by AlexNet is reduced using autoencoders.

In the deep AIS version, in order to reduce dimensionality of the AlexNet feature vector and simultaneously increase the level of characteristics, two autoencoders are used. The input layer of the first autoencoder receives the training vectors, each one with 4096 characteristics. After finishing the first autoencoder training process, the output provided by the hidden layer of the first autoencoder is used as input to the second autoencoder. After its training process, the second autoencoder returns the deep features vector (green part of the whole vector in Figure 9) as its output. The feature vector is then joined with AIS features (blue part of the whole feature vector in Figure 9).

V. EXPERIMENTS

A. MATERIALS

Twenty computerized radiographic images of welded joints were used in the experiments - all obtained by the GE or Dürr

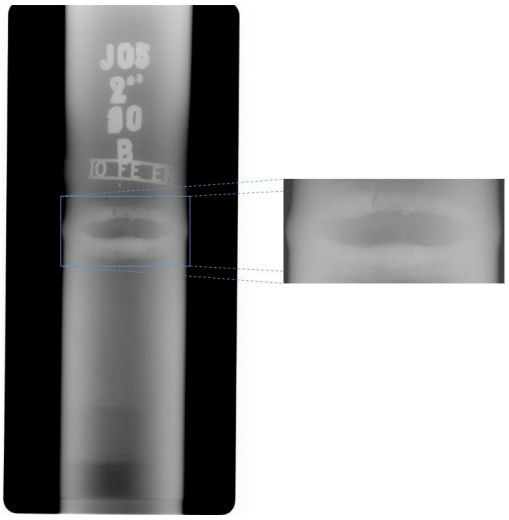

FIGURE 14. Image of the pipe, highlighting the weld bead clipping.

computer radiography systems. All images are taken by the 65,536 grayscales (16 bpp) DWDI technique and are obtained from actual operating conditions. Consequently, they are affected by different capture and scanning parameters, such as amount of radiation and exposure time, leading to different levels of brightness, noise, and contrast. Figure 14 shows one of the weld bead clipping extracted from the pipe and used in the training of the proposed systems.

As reported by experts, the most frequent discontinuities of welded joint defects are: cracks (CR), lack of fusion (LF), lack of penetration (LP), undercut (UC), slag inclusion (SI), and porosity (PO). Figure 15(b) shows the report of image depicted in Figure 15(a) manually processed by the laudist, in which the presence of defects porosity and inclusion of tungsten is highlighted.

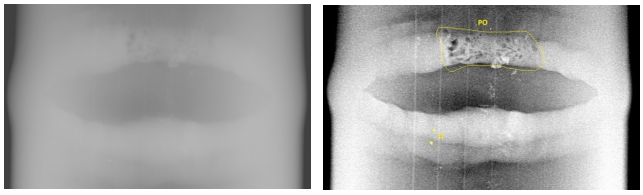

(a) (b)

FIGURE 15. Images of the weld bead. (a) Cropping the original image. (b) Report with defects identified on the image manually processed by the laudist.

B. DEEP AIS PARAMETERS

Based on the detected discontinuities, an image bank was structured containing 727 discontinuities, out of which 362 samples are instances of non-defects, and 365 samples are instances of defects. To detect and identify discontinuities in each image, digital processing techniques are used, such (i) as filters for noise removal (average, median, Gaussian and Wiener) or smoothing, (ii) morphological image processing (erosion, dilation, top-hat transformation and bottom-hat transformation), (iii) thresholding (Otsu and adaptive thresholding), sharpening and labeling. Although important, this pre-processing phase is out of the scope of the paper since this phase has been extensively investigated in a previous work [24]. Notice that the amount of discontinuities obtained in each image can different, therefore for some images there might be few discontinuities and for others this total can be large. Since most of discontinuities represent non-defects, aiming to provide a balanced dataset only 362 examples of non-defects were chosen considering discontinuities with sizes and shape similar to defect discontinuities but with different textures.

In the experiments performed in the present paper, the same 13 geometric and texture features used in Boaretto's work [26] are considered (area, extent, ratio 1, ratio 2, ratio 3, rounding, eccentricity, solidity, difference, contrast, standard deviation, entropy, and asymmetry). Moreover, 100 features obtained from the output of the second autoencoder in the deep learning module are added to the 13 features (geometry and texture), totaling 113 features in the whole vector considered in the proposed deep AIS. Different from the feature maps that occur in the first layers of a Convolutional Neural Network (CNN) and usually provide images with interpretable representation, the 100 features extracted from the output of the second auto-encoder have no interpretable meaning. They are only values representing a sequence of space transformations performed by AlexNet (4096 features) + Autoencoder1 (1000 features) + Autoencoder2 (100 features).

Table 1 presents parameters and values used in deep AIS.

TABLE 1. | Parameters and values.

Parameters	Value	Detailed description
γ_s	0.99	Set threshold value in sensoring phase
γ_d^0	0.96	Initial defect threshold used in the monitoring phase
γ_d^c	{0.99, 0.98, 0.97, 0.96, 0.95, 0.90, 0.85, 0.80, 0.75, 0.70, 0.60, 0.50}	Dynamic defect threshold values tested in clonal selection phase
C	4	Total cycles of evolution
G	25	Maximum Generation per Cycle
MaxGeneration	C*G	-
[-M, M]	{-3, -2,…,2, 3}	Range of MO operator
|SE|	4	Total of SE types

The size of antibody population $|P_{Ab}|$ is a parameter set according to the total number of cells resulting after NSA algorithms.

In the experiments, it is assumed that the affinity value f of antibody i is within the range [0.0,1.0] using d = Euclidean distance. The number of clones (n) generated from each antibody is based on the affinity value f_i. Regarding the hypermutation rate, the antibody detector genes undergo one modification from the current gene if ($f_\mathbf{i} \geq 0.5$) and two modifications if ($f_\mathbf{i} < 0.5$).

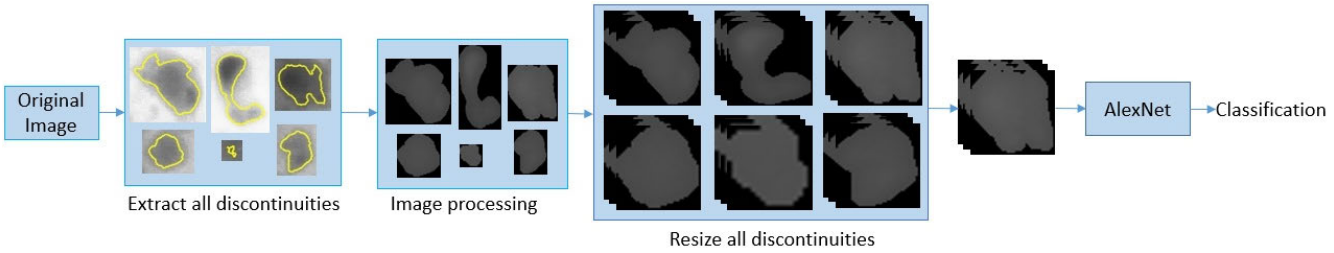

FIGURE 16. CNN method - AlexNet.

C. COMPARISON APPROACHES

The deep AIS system consists of two modules: AIS and deep learning. Therefore, to emphasize the need for the hybrid approach proposed, the pure AIS system and the pure deep learning system are considered as comparison approaches.

The pure AIS system considers only the AIS module (Figure 8) to classify the discontinuities.

The pure deep system is illustrated in Figure 16 and considers only the AlexNet to classify the discontinuities detected in the pre-processing phase.

As explained in section II.C.2, the AlexNet network is a 25-layer deep learning model used to classify 1000 classes (categories). However, it is possible to classify another group of images with a different number of classes (categories). To this end, the last three layers are adjusted for the new classification problem. The pre-trained CNN is adapted to our dataset using a fine-tuning technique in which the weights of the convolutional part of the pre-trained CNN are frozen, and only the last three layers of the AlexNet are trained. These layers are trained with input images of size $227\times227\times3$ (see Figure 16 for more details) using the Stochastic Gradient Descent (SGD) algorithm and the sigmoid activation function [29].

In this paper, the last three layers of AlexNet (layers 23, 24, and 25) are adjusted according to the method described in [62] – [65]. For layer 23 (Fully Connected) the new layer options are specified to have the number of classes of the new problem, which, in this case, are two classes for the discontinuities (defect and non-defect).

VI. RESULTS AND DISCUSSIONS

This section discusses the results obtained by the deep AIS approach proposed for the classification of discontinuities into defects and non-defects. Moreover, the proposal is compared with standalone versions of AIS and deep learning.

The first procedure is performed in the pre-processing phase: detecting the discontinuities in weld bead clipping images through the approach described in Boaretto [26]. Figure 17 presents the results of pre-processing for one of the images, in which detected discontinuities are highlighted.

With all discontinuities detected, the whole data set is divided into three sets: training (50%), validation (25%), and test (25%). The training phase of the proposed approach encompasses the definition of the self and nonfself data in the AIS module as well as training the deep models. The validation set is used to tune some parameters of each model when subjected to a controlled test. Finally, the test set is used to effectively evaluate the approaches when classifying defect or non-defect discontinuities, with the parameters fixed with values defined in the validation phase.

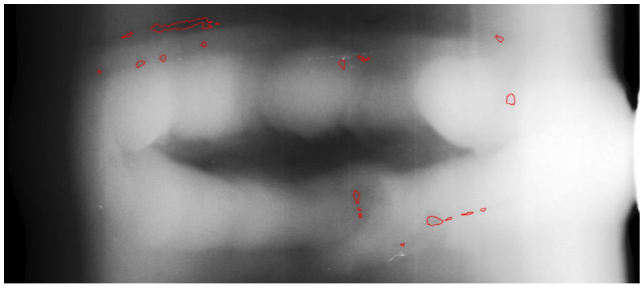

FIGURE 17. Detection of discontinuities to be used by all the approaches.

A. VALIDATION PHASE

1) PURE AND DEEP AIS PARAMETER TUNING

Despite the fact many parameters present in the Deep AIS approach were empirically set (especially those regarding the deep models), this section aims to investigate the values of γ_d^c used in each cycle of the AIS module, since it was observed that there was a high sensibility of this module to this parameter.

One must have in mind that, after the pre-processing phase, identified discontinuities are evaluated by negative selection in NSA aiming to separate, among all discontinuities, those that are clearly non-defects. The affinity between feature vectors of each T cell and the bank of self cells is calculated and compared with γ_s (set as 0.99 according to Table 1). By setting a high value, only discontinuities strongly characterized as non-defects are classified as self, labeled in the original image, and eliminated from the process. Therefore, only possible defects remain for future analysis.

Subsequently, cells representing possible defects are compared with nonself cells. In this recognition process, the matching between feature vectors is calculated and compared with an initial defect threshold (γ_d^0) set in the first step of the monitoring phase. It is important to emphasize that the main objective of this paper is to propose a method for detecting defects by verifying the effectiveness of artificial

immune systems in the repertoire evolution instead of classifying all discontinuities at the beginning of the process. Then, in nonself matching, the threshold is initially set with a high value ($\gamma_d^0 = 0.99$). In nonself classification, cells classified as defect (affinity with antigens $> \gamma_d^0$) have their discontinuities labeled in the original image and leave the process. The remaining cells undergo clonal selection.

In each generation of CSA, the affinity between Ab and Ag is compared with a dynamic threshold γ_d^c. Different values were tested for the update of γ_d^c value: 0.99, 0.98, 0.97, 0.96, 0.95, 0.90, 0.85, 0.80, 0.75, 0.70, 0.60, and 0.50.

Aiming to define how evolution occurs considering different values for the static threshold (γ_d), each value was tested by setting it and running AIS with this value fixed from the beginning until the end (i.e. from 1 to C*G generations). Figure 18 shows the performance (Fscore in y axis) achieved for each tested value of γ_d(axis x). One observes that a) there is room for improvements in performance by decreasing threshold values; b) there are four different levels of performances: one with $\gamma_d = \gamma_d^0$, and three others (level 1 in blue, level 2 in green, and level 3 in yellow). Thus, it was decided to divide the whole evolutionary process into four cycles (each one running for G generations with a different value of γ_d). During the tuning phase, different combinations of values were tested to update parameter γ_d^c. The conclusion was that the set $\gamma_d = \{0.97$ (for c=1), 0.90 (for c = 2), 0.85 (for c = 3), and 0.75 (for c = 4)$\}$ achieves a good compromise between accuracy and sensibility measured by the Fscore metric. Therefore, these values were chosen to be used in the standard versions of pure AIS and deep AIS approaches considered in the following section.

FIGURE 18. Fscore for each single threshold value mainted fixed along all G generations.

2) ALEXNET PARAMETER TUNING

AlexNet is used to classify defects or non-defects from discontinuities in weld bead images, with some modifications from its original configuration. Ten rounds are performed with different randomly determined initial weights. Figure 19 illustrates the values obtained during the training. The best model was chosen as the standard version of the pure deep model.

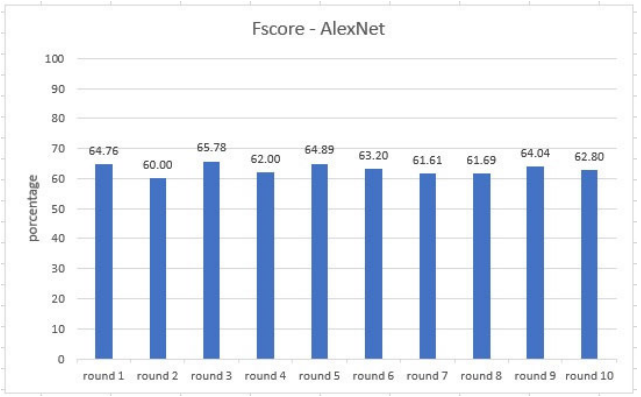

FIGURE 19. Training Fscore of each round obtained by AlexNet.

B. PERFORMANCE COMPARISONS

In this section, discontinuities in the output image are color-coded: the defect-classified discontinuities are shown in green, and discontinuities classified as non-defects are shown in yellow. Aiming to compare the classification performed by all the comparison approaches with the identification performed by the experts, the manually reported image is inserted in the lower left corner for each comparison approach.

An example of the two-class pure AIS classifier output image (defect and non-defect) can be seen in Figure 20 (right). For this image, out of 19 pre-processed discontinuities, seven discontinuities are misclassified, five are classified as defects (false positives), and two defects are classified as non-defects (false negatives), according to the reported image.

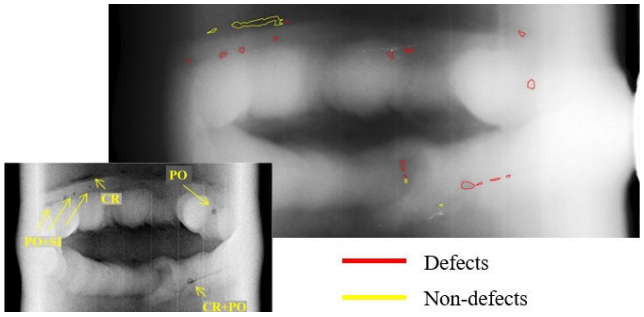

FIGURE 20. Image after the classification of discontinuities. Image obtained from pure AIS classifier and report of inspection provided by an expert.

An example of the two-class deep AIS classifier output image (defect and non-defect) can be seen in Figure 21 (right). For this image, out of 19 pre-processed discontinuities in the image, five discontinuities are not classified correctly: four false positives and one false negative, as can be observed in the reported image.

An example of an AlexNet output image for both classes (defect and non-defect) can be seen in Figure 22. For this image, out of 19 pre-processed discontinuities, six

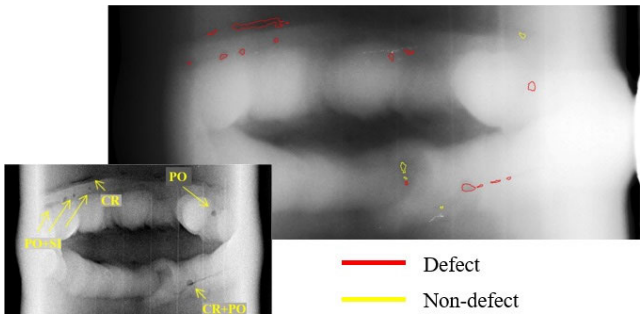

FIGURE 21. Image after the classification of discontinuities. Image obtained by Deep AIS classifier and report of inspection provided by an expert.

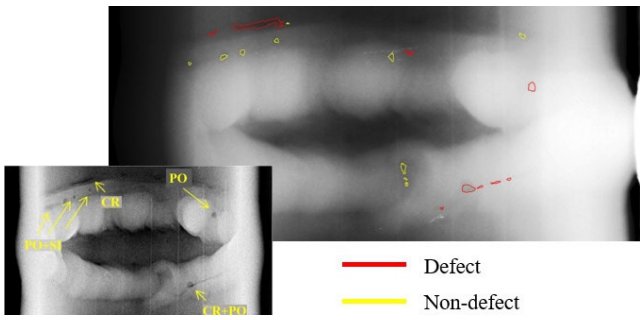

FIGURE 22. Image after the classification of discontinuities. Image obtained by AlexNet-based classifier and report of inspection provided by an expert.

discontinuities are not classified correctly - two false positives and five false negatives - as can be observed with the reported image. Despite the difference of only on error, AlexNet provided five false negatives, which might be more dangerous than false positives.

Analyzing the Fscore criteria obtained for each of the three methods (Figure 23), one observes that AlexNet had the poorest performance, with an Fscore of 64.86%, while the proposed approach obtained the best performance, with an Fscore of 70.732%, obtaining a gain of 4.356% over pure AIS, the Fscore of which is 66.376%.

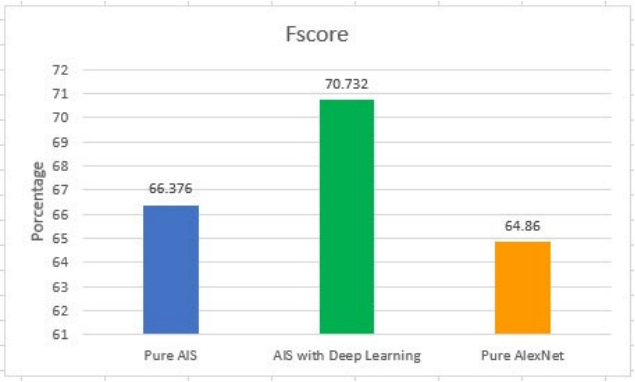

FIGURE 23. Best Fscore obtained by each method.

One hypothesis for the poor AlexNet performance can be the small available training set. Since CNN are supposed to work well under large training sets, we can conclude that for this application CNN might not be suitable to perform the whole classification task.

In addition to the best Fscore, the Deep AIS classifier obtained - in the training phase - the lowest false negative rate (FN) when compared to other approaches presented in the current article, as can be observed in Figure 24. In the present case, the lower FN value indicates that there are few samples incorrectly classified as not belonging to the defect class.

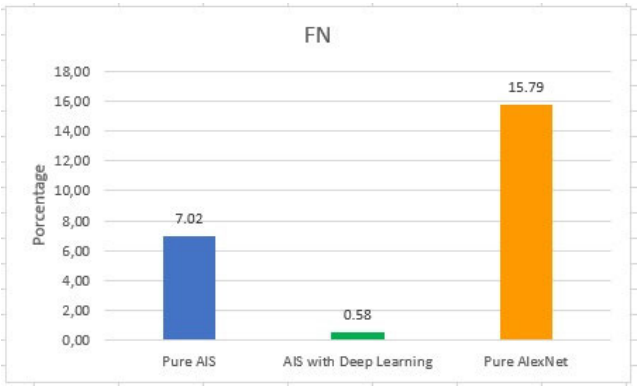

FIGURE 24. Best FN obtained by each method.

Another interesting finding appears when the results achieved by the standard versions of AIS (pure and deep) are compared with those achieved by versions using fixed thresholds. Thus, one concludes that adopting a dynamic threshold that decreases its values as long as evolution occurs is beneficial to the AIS module since both dynamic versions outperform their static counterparts, even those with the lowest static values.

VII. CONCLUSION

The main idea behind the approach proposed in this paper is the attempt to reproduce the way a human being inspects radiographic images, inspired by the functioning mechanism of the biological immune system. First, it pre-processes the image investigating the regions of attention (discontinuities). Then, it separates discontinuities that can be clearly classified as non-defects (self cells) and defects (nonself cells). Then the system starts a process aiming to 1) improve the non-classified data by means of lenses-like transformation performed by antibodies evolution, and 2) reduce, from time to time, the threshold value necessary to classify a discontinuity as a defect aiming to reduce the false negative rates as much as possible. Experiments were performed with DWDI radiographic images obtained in real field situations and which, in most cases, present images of a lower quality when compared to those used in other studies.

The proposed approach (deep AIS) uses a CNN AlexNet plus an autoencoder incorporated into the AIS module. AlexNet is used aiming to extract other features

TABLE 2. AlexNet layers.

Number	Description	Detailing
1	Image input	227x227x3 images with 'zerocenter' normalization
2	Convolution	96 11x11x3 convolutions with stride [4 4] and padding [0 0 0 0]
3	Reread	Reread
4	Cross Channel Normalization	cross channel normalization with 5 channels per element
5	Maxpooling	3x3 maxpooling with stride [2 2] and padding [0 0 0 0]
6	Convolution	256 5x5x48 convolutions with stride [1 1] and padding [2 2 2 2]
7	Reread	Reread
8	Cross Channel Normalization	cross channel normalization with 5 channels per element
9	Maxpooling	3x3 max pooling with stride [2 2] and padding [0 0 0 0]
10	Convolution	384 3x3x256 convolutions with stride [1 1] and padding [1 1 1 1]
11	Reread	Reread
12	Convolution	384 3x3x192 convolutions with stride [1 1] and padding [1 1 1 1]
13	Reread	Reread
14	Convolution	256 3x3x192 convolutions with stride [1 1] and padding [1 1 1 1]
15	Reread	Reread
16	Maxpooling	3x3 max pooling with stride [2 2] and padding [0 0 0 0]
17	Fully Connected	4096 fully connected layer
18	Reread	Reread
19	Dropout	50% dropout
20	Fully Connected	4096 fully connected layer
21	Reread	Reread
22	Dropout	50% dropout
23	Fully Connected	1000 fully connected layer
24	Softmax	softmax
25	Classification Output	crossentropyex with 'tench' and 999 other classes

that are added to the geometric and texture features to improve classification. The autoencoder is used to reduce the number of features extracted by AlexNet to 100 features considered in the present work.

This paper compared the proposed approach with two other methods (pure AIS and a deep learning approach - AlexNet) for automatic defect detection in oil pipe welds. This comparison aimed to answer the question: is it really necessary to adopt a hybrid approach to perform this task?

The answer is yes, since the standard version of the proposed approach achieves an Fscore of 70.732%, outperforming the pure AIS (Fscore = 66.376%) and AlexNet used to perform the entire process (Fscore of 64.86%). This poorest result of the pure deep learning model is probably due to the low cardinality of training set, even with the use of transfer learning, but further investigation is necessary to confirm this. It is important to point out that, with the worst Fscore results, AlexNet obtained the highest FN value, indicating that many discontinuities that belong to the defect class were classified as non-defects; which is a huge problem in the considered classification context. On the other hand, the hybrid version outperformed the others not only in terms of Fscore, but also with the lowest FN value.

Besides their better results, another advantage of AIS models is their online learning capabilities. Different from CNN models, which require hard retraining processes, incorporating new information into the self and nonself banks is quite easy for AIS models. As long as new detected discontinuities are classified as self and nonself with a high level of confidence, they can be easily incorporated into the self repository and antigen banks, and new discontinuities could take advantage of this new information.

From the conducted experiments, one can conclude that, using the proposed approach, it was possible to automatically identify the discontinuities and classify the discontinuities into defects and non-defects, highlighting the result in the image. The resulting image helps the expert in preparing technical reports.

With the obtained results, new perspectives emerge to be explored in this field, like the analysis and / or incorporation of other methods for extracting the features; incorporation of other artificial intelligence methods (including other CNN models) into the pure AIS method, as it performed relatively well when used in a standalone mode. Another topic is the exploration of the online learning capability of the AIS module.

APPENDIX

see Table 2.

ACKNOWLEDGMENT

The authors would like to thank the radiographies provided by Leopoldo Américo Miguez de Mello Research and Development Center (Cenpes)-Brazilian Petroleum (Petrobras).

REFERENCES

[1] M. L. Nayyar, *Piping Handbook*. New York, NY, USA: McGraw-Hill, 1992.

[2] M. K. Felisberto, H. S. Lopes, T. M. Centeno, and L. V. R. de Arruda, "An object detection and recognition system for weld bead extraction from digital radiographs," *Comput. Vis. Image Understand.*, vol. 102, no. 3, pp. 238–249, 2006.

[3] H. Jagannathan, N. Bhaskar, P. C. N. Sriraman, and N. A. Vijay, "A step towards automatic defect pattern analysis and evaluation in industrial radiography using digital image processing," in *Proc. 15th World Conf. Non Destructive Test.*, Rome, Italy, Oct. 2000, pp. 15–21.

[4] ASNT. (2017). *Introduction to Nondestructive Testing*. Accessed: Aug. 2017. [Online]. Available: https://www.asnt.org/MinorSiteSections/AboutASNT/Intro-to-NDT.aspx

[5] W. C. Godoi, R. R. da Silva, and V. Swinka-Filho, "Pattern recognition in the automatic inspection of flaws in polymeric insulators," *Insight-Non-Destructive Test. Condition Monit.*, vol. 47, no. 10, pp. 608–614, 2005.

[6] S. W. Lawson and G. A. Parker, "Intelligent segmentation of industrial radiographic images using neural networks," *Proc. SPIE*, vol. 2347, pp. 245–255, Oct. 1994.

[7] G. Wang and T. W. Liao, "Automatic identification of different types of welding defects in radiographic images," *NDT & E Int.*, vol. 35, no. 8, pp. 519–528, 2002.

[8] R. R. da Silva, M. H. S. Siqueira, M. P. V. de Souza, J. M. A. Rebello, and L. P. Calôba, "Estimated accuracy of classification of defects detected in welded joints by radiographic tests," *NDT & E Int.*, vol. 38, no. 5, pp. 335–343, 2005.

[9] H. I. Shafeek, E. S. Gadelmawla, A. A. Abdel-Shafy, and I. M. Elewa, "Assessment of welding defects for gas pipeline radiographs using computer vision," *NDT & E Int.*, vol. 37, no. 4, pp. 291–299, 2004.

[10] G. X. Padua, R. R. da Silva, M. H. S. Siqueira, J. M. A. Rebello, L. P. Caloba, and R. de Janeiro, "Classification of welding defects in radiographs using traversal profiles to the weld seam," in *Proc. 16th World Conf. Nondestruct. Test.*, 2004.

[11] S. M. Alghalandis and G. H. N. Alamdari, "Welding defect pattern recognition in radiographic images of gas pipelines using adaptive feature extraction method and neural network classifier," in *Proc. 23rd World Gas Conf.*, Amsterdam, The Netherlands, 2006, pp. 1–13.

[12] T. W. Liao, "Classification of weld flaws with imbalanced class data," *Expert Syst. Appl.*, vol. 35, no. 3, pp. 1041–1052, 2008.

[13] G. Liling and Z. Yingjie, "Hierarchical segmentation approach to detection of defects on welding radiographic images," in *Proc. 4th IEEE Conf. Ind. Electron. Appl. (ICIEA)*, May 2009, pp. 2089–2094.

[14] A. Mahmoudi and F. Regragui, "Fast segmentation method for defects detection in radiographic images of welds," in *Proc. IEEE/ACS Int. Conf. Comput. Syst. Appl. (AICCSA)*, May 2009, pp. 857–860.

[15] A. Mahmoudi and F. Regragui, "Welding defect detection by segmentation of radiographic images," in *Proc. WRI World Congr. Comput. Sci. Inf. Eng.*, Mar./Apr. 2009, pp. 111–115.

[16] I. Valavanis and D. Kosmopoulos, "Multiclass defect detection and classification in weld radiographic images using geometric and texture features," *Expert Syst. Appl.*, vol. 37, no. 12, pp. 7606–7614, 2010.

[17] J. Zapata, R. Vilar, and R. Ruiz, "An adaptive-network-based fuzzy inference system for classification of welding defects," *NDT & E Int.*, vol. 43, no. 3, pp. 191–199, 2010.

[18] N. B. Yahia, T. Belhadj, S. Brag, and A. Zghal, "Automatic detection of welding defects using radiography with a neural approach," *Procedia Eng.*, vol. 10, pp. 671–679, 2011.

[19] W. Chen, Z. Miao, and D. Ming, "Automated inspection using X-ray imaging," in *Proc. IEEE 10th Int. Conf. Trust, Secur. Privacy Comput. Commun. (TrustCom)*, Nov. 2011, pp. 1769–1772.

[20] D. Mery, "Automated detection of welding discontinuities without segmentation," *Mater. Eval.*, vol. 69, no. 6, pp. 656–663, 2011.

[21] S. A. Halim, N. A. Hadi, A. Ibrahim, and Y. H. P. Manurung, "The geometrical feature of weld defect in assessing digital radiographic image," in *Proc. IEEE Int. Conf. Imag. Syst. Techn. (IST)*, May 2011, pp. 189–193.

[22] S. A. Halim, A. Ibrahim, M. I. Jayes, and Y. H. P. Manurung, "Weld defect features extraction on digital radiographic image using Chan–Vese model," in *Proc. IEEE 9th Int. Colloq. Signal Process. Appl. (CSPA)*, Mar. 2013, pp. 67–72.

[23] V. R. Rathod and R. S. Anand, "A comparative study of different segmentation techniques for detection of flaws in NDE weld images," *J. Nondestruct. Eval.*, vol. 31, no. 1, pp. 1–16, 2012.

[24] M. Kroetz, T. M. Centeno, M. R. Delgado, M. Felisberto, L. A. Lucas, L. B. Dorini, V. Fylyk, and A. Vieira, "Genetic algorithms to automatic weld bead detection in double wall double image digital radiographs," in *Proc. IEEE Congr. Evol. Comput.*, Jun. 2012, pp. 1–7.

[25] F. M. Suyama, A. G. Krefer, A. R. Faria, and T. M. Centeno, "Detecting central region in weld beads of DWDI radiographic images using PSO," *Int. J. Natural Comput. Res.*, vol. 5, no. 1, pp. 42–56, 2015.

[26] N. Boaretto and T. M. Centeno, "Automated detection of welding defects in pipelines from radiographic images DWDI," *NDT & E Int.*, vol. 86, pp. 7–13, Mar. 2017.

[27] R. Miranda, M. Delgado, T. Mezzadri, R. D. da Silva, M. Vaz, and C. Marinho, "WBdetect: Particle swarm optimization for segmenting weld beads in radiographic images," in *Designing with Computational Intelligence*. Cham, Switzerland: Springer, 2017, pp. 217–236.

[28] F. M. Suyama, M. R. Delgado, R. D. da Silva, and T. M. Centeno, "Deep neural networks based approach for welded joint detection of oil pipelines in radiographic images with double wall double image exposure," *NDT & E Int.*, vol. 105, pp. 46–55, Jul. 2019.

[29] K. L. Wiggers, A. S. Britto, L. Heutte, A. L. Koerich, and L. E. S. Oliveira, "Document image retrieval using deep features," in *Proc. Int. Joint Conf. Neural Netw. (IJCNN)*, Jul. 2018, pp. 1–8.

[30] F. Zhuang, X. Cheng, P. Luo, S. J. Pan, and Q. He, "Supervised representation learning: Transfer learning with deep autoencoders," in *Proc. 24th Int. Joint Conf. Artif. Intell. (IJCAI)*, Buenos Aires, Argentina, 2015, pp. 4119–4125.

[31] J. Yosinsk, J. Clune, Y. Bengio, and H. Lipson, "How transferable are features in deep neural networks?" in *Proc. Adv. Neural Inf. Process. Syst.*, Z. Ghahramani, Ed., 2014, pp. 3320–3328.

[32] M. Oquab, L. Bottou, I. Laptev, and J. Sivic, "Learning and transferring mid-level image representations using convolutional neural networks," in *Proc. IEEE Conf. Comput. Vis. Pattern Recognit.*, Jun. 2014, pp. 1717–1724.

[33] *ASME Boiler & Pressure Vessel Code*, Section V, Subsection A, Article 2, Nonmandatory Appendices, Appendix A, Amer. Soc. Mech. Eng., New York, NY, USA, 2004, pp. 34–37.

[34] P. C. Berbert, L. J. R. F. Filho, T. A. Almeida, M. B. Carvalho, and A. Yamakami, "Artificial immune system to find a set of k-spanning trees with low costs and distinct topologies," in *Proc. Int. Conf. Artif. Immune Syst.* Berlin, Germany: Springer, 2007, pp. 395–406.

[35] A. B. S. Serapião, J. R. P. Mendes, and K. Miura, "Artificial immune systems for classification of petroleum well drilling operations," in *Proc. Int. Conf. Artif. Immune Syst.* Berlin, Germany: Springer, 2007, pp. 47–58.

[36] D. Dasgupta, "Advances in artificial immune systems," *IEEE Comput. Intell. Mag.*, vol. 1, no. 4, pp. 40–49, Nov. 2006.

[37] S. Forrest, A. S. Perelson, L. Allen, and R. Cherukuri, "Self-nonself discrimination in a computer," in *Proc. IEEE Comput. Soc. Symp. Res. Secur. Privacy*, May 1994, pp. 202–212.

[38] D. Dasgupta and F. Gonzalez, "Artificial immune systems in intrusion detection," *Enhancing Comput. Secur. Smart Technol.*, vol. 1, pp. 165–208, Jun. 2005.

[39] L. N. de Castro and F. J. Von Zuben, "Artificial immune systems: Part I—Basic theory and applications," Dept. Comput. Eng. Ind. Automat., Fac. Elect. Comput. Eng., State Univ. Campinas, Campinas, Brazil, Tech. Rep. RT DCA 01/99, 1999, vol. 210, no. 1.

[40] L. N. de Castro and J. Timmis, *Artificial Immune Systems: A New Computational Intelligence Approach*. New York, NY, USA: Springer, 2002.

[41] L. N. de Castro and F. J. Von Zuben, "The clonal selection algorithm with engineering applications," in *Proc. GECCO*, 2000, pp. 36–39.

[42] B. C. Yavuz, N. Yurtay, and O. Ozkan, "Prediction of protein secondary structure with clonal selection algorithm and multilayer perceptron," *IEEE Access*, vol. 6, pp. 45256–45261, 2018.

[43] Y. Zhong and L. Zhang, "Sub-pixel mapping based on artificial immune systems for remote sensing imagery," *Pattern Recognit.*, vol. 46, no. 11, pp. 2902–2926, 2013.

[44] L. N. de Castro and F. J. Von Zuben, "Learning and optimization using the clonal selection principle," *IEEE Trans. Evol. Comput.*, vol. 6, no. 3, pp. 239–251, Jun. 2002.

[45] Y. Lecun, "Generalization and network design strategies," *Connectionism in Perspective*. Zurich, Switzerland: Elsiever, 1989.

[46] S. Haykin, *Neural Networks and Learning Machines*, vol. 3. Upper Saddle River, NJ, USA: Pearson, 2009.

[47] A. Krizhevsky, I. Sutskever, and G. E. Hinton, "ImageNet classification with deep convolutional neural networks," in *Proc. Adv. Neural Inf. Process. Syst.*, 2012, pp. 1097–1105.

[48] A. Kartaphy, F. F. Li, and J. Johnson, "CS231n: Convolutional neural networks for visual recognition," *Neural Netw.*, vol. 1, 2016. [Online]. Available: http://cs231n.github.io

[49] U. Karn. (2016). *An Intuitive Explanation of Convolutional Neural Networks. The Data Science Blog*. [Online] Available: https://ujjwalkarn.me/2016/08/11/intuitive-explanation-convnets/.

[50] I. GoodFellow, Y. Bengio, and A. Courville, *Deep Learning*. Cambridge, MA, USA: MIT Press, 2016. [Online]. Available: http://www.deeplearningbook.org

[51] S. Haykin, *Neural Networks and Learning Machines*, vol. 3. Upper Saddle River, NJ, USA: Pearson, 2009.
[52] S. Lu, Z. Lu, and Y. Zhang, "Pathological brain detection based on AlexNet and transfer learning," *J. Comput. Sci.*, vol. 30, pp. 41–47, Jan. 2019.
[53] X. Han, Y. Zhong, L. Cao, and L. Zhang, "Pre-trained alexnet architecture with pyramid pooling and supervision for high spatial resolution remote sensing image scene classification," *Remote Sens.*, vol. 9, no. 8, p. 848, 2017.
[54] D. Priori, "Comparison of neural network models applied to size prediction of atmospheric particles based on their two-dimensional light scattering patterns," M.S. thesis, Federal Univ. Santa Catarina, Florianópolis, Brazil, 2017.
[55] B. Li, F. Sun, and Y. Zhang, "Building recognition based on sparse representation of spatial texture and color features," *IEEE Access*, vol. 7, pp. 7220–7227, 2019.
[56] Y. Bengio, "Learning deep architectures for AI," *Found. Trends Mach. Learn.*, vol. 2, no. 1, pp. 1–127, 2009.
[57] R. C. Gonzalez and R. E. Woods, *Digital Image Processing*. Upper Saddle River, NJ, USA: Prentice-Hall, 2008.
[58] M. Sokolova and G. Lapalme, "A systematic analysis of performance measures for classification tasks," *Inf. Process. Manage.*, vol. 45, no. 4, pp. 427–437, 2009.
[59] D. M. Powers, "Evaluation: From precision, recall and F-measure to ROC, informedness, markedness and correlation," *J. Mach. Learn. Technol.*, vol. 2, no. 1, pp. 37–63, Feb. 2011.
[60] N. Nacereddine and M. Tridi, "Computer-aided shape analysis and classification of weld defects in industrial radiography based invariant attributes and neural networks," in *Proc. 4th Int. Symp. Image Signal Process. Anal. (ISPA)*, Sep. 2005, pp. 88–93.
[61] H. Yazid, H. Arof, H. Yazid, S. Ahmad, A. A. Mohamed, and F. Ahmad, "Discontinuities detection in welded joints based on inverse surface thresholding," *NDT & E Int.*, vol. 44, no. 7, pp. 563–570, 2011.
[62] S. Park, F. Pan, S. Kang, and C. D. Yoo, "Driver drowsiness detection system based on feature representation learning using various deep networks," in *Proc. Asian Conf. Comput. Vis.* Cham, Switzerland: Springer, 2016, pp. 154–164.
[63] W. Nawaz, S. Ahmed, A. Tahir, and H. A. Khan, "Classification of breast cancer histology images using ALEXNET," in *Proc. Int. Conf. Image Anal. Recognit.* Cham, Switzerland: Springer, 2018, pp. 869–876.
[64] P. Oza and V. M. Patel, "One-class convolutional neural network," *IEEE Signal Process. Lett.*, vol. 26, no. 2, pp. 277–281, Feb. 2018.
[65] L. Xiao, Q. Yan, and S. Deng, "Scene classification with improved AlexNet model," in *Proc. 12th Int. Conf. Intell. Syst. Knowl. Eng. (ISKE)*, Nov. 2017, pp. 1–6.

CELIA CRISTINA BOJARCZUK FIORAVANTI received the B.S. degree in computer engineering from the Pontifical Catholic University of Paraná (PUCPR), in 1996, and the M.S. degree in electrical and computer engineering from the Federal University of Technology–Paraná, Brazil, in 2001, where she is currently pursuing the Ph.D. degree with the Graduate Program in Electrical and Computer Engineering. She has been a Full Professor with the Department of Electrical Engineering, Federal University of Technology of Paraná, since 1997. Her main interests are computer vision, pattern recognition, digital image processing, and computational intelligence.

TANIA MEZZADRI CENTENO received the B.S. degree in computer science and the M.S. degree in electrical and computer engineering from the Federal University of Technology-Paraná, in 1985 and 1994, respectively, and the Ph.D. degree in computer science from the Université Paul Sabatier de Toulouse II, in 1998. She has been a member of the Department of Informatics, Federal University of Technology-Paraná, since 1991. She received the Research Fellowship from the National Council for Scientific and Technological Development (CNPq). She also received the financial support for research projects from a number of funding agencies. Her main interests are computer vision, pattern recognition, and digital image processing.

MYRIAM REGATTIERI DE BIASE DA SILVA DELGADO received the graduate degree in electrical engineering from the Federal University of Goiás, in 1990, and the M.S. degree in electric engineering and the Ph.D. degree in computer engineering from the State University of Campinas, in 1993 and 2002, respectively. She is currently a Full Professor of electrical and computer engineering with the Department of Informatics and Graduate Program, Federal University of Technology of Paraná, Brazil. Her research interests include computational intelligence applied to the areas of optimization and logistics, image processing, mobile device networks, and bioinformatics.